Antiviral and Antibacterial Cold Spray Coating Application on Rubber Substrate, Disruption in Disease Transmission Chain

D. C. Saha[1] · S. J. Boegel[2] · S. Tanvir[2] · C. L. Nogueira[2] · M. G. Aucoin[2] ·
W. A. Anderson[2] · H. Jahed[1] (ORCID)

Abstract The objective of this study was to prepare a copper-coated rubber surface using cold spray technology with improved virucidal and antimicrobial properties to fight against highly transmissible viruses and bacteria. A successful cold spray coating was produced using irregular-shaped pure Cu powder on an escalator handrail rubber. The powder particles and the deposited coatings (single and double pass) were characterized in terms of particle morphology and size distribution, coating surface and coat/substrate cross-section properties. The bonding between powder and rubber surfaces was purely mechanical interlocking. The Cu powder penetration depth within the rubber surface increases with a number of depositions pass. The virucidal properties of the coated surface were tested utilizing surrogates for SARS-CoV-2: HCoV-229E, a seasonal human coronavirus, and baculovirus, a high-titer enveloped insect cell virus. A double-pass coated surface showed significant baculovirus inactivation relative to a bare rubber control surface after 2-h (approximately 1.7-log) and 4-h (approximately 6.2-log), while a 4-h exposure reduced HCoV-229E titer to below the limit of detection. A similar microbial test was performed using *E. coli,* showing a 4-log microbial reduction after 2-h exposure relative to the bare rubber. These promising results open a new application for cold spray in the health sector.

Keywords bonding mechanism · cold spray · copper powder · rubber substrate · viricidal test, antimicrobial test, contact inactivation

This article is part of a special topical focus in the Journal of Thermal Spray Technology on New and Emerging Markets in Thermal Spray. The issue was organized by Dr. Andrew Vackel, Sandia National Laboratories; Dr. John Koppes, TST Engineered Coating Solutions; Prof. Bertrand Jodoin, University of Ottawa; Dr. Dheepa Srinivasan, Pratt and Whitney; and Prof. Shrikant Joshi, University West.

✉ H. Jahed
hamid.jahed@uwaterloo.ca

1   Fatigue and Stress Analysis Laboratory, Department of Mechanical & Mechatronics Engineering, University of Waterloo, 200 University Avenue West, Waterloo, ON N2L 3G1, Canada

2   Department of Chemical Engineering, University of Waterloo, Waterloo, ON N2L 3G1, Canada

Introduction

Copper and its alloys have shown orders of magnitude better antimicrobial properties than other commonly used metals and polymers (Ref 1). There is some anecdotal evidence that copper has similar properties in fighting the human coronavirus in general (Ref 2), by rapid inactivation, irreversible destruction, and massive structural damage of the virus when it is exposed to copper alloys; and particularly in disabling SARS-CoV-2, the novel coronavirus causing COVID-19 (Ref 3). In a recent study (Ref 3) by the Centers for Disease Control (CDC), the decay rates of SARS-CoV-2 virus on pure copper (99.9%) surfaces were shown to be much faster (an order of magnitude) than on stainless steel and an extra twofold faster than that on plastic surfaces. Most shared public surfaces are made of metals (e.g., steel, and aluminum) and plastics (e.g., PVC, composites, rubber). Handrails, seats, doorknobs, shopping carts, and door handles are examples of commonly shared surfaces in public transportation, parks, and malls that are touched by hands. If the disinfection rate of the surfaces is increased, the chance of transmission of active bacteria and viruses is reduced considerably.

The mechanisms by which the copper ions attack the cell membrane and influx into the internal structures are still a matter of research. Although the exact mechanism of contact-killing is yet to be discovered, Grass et al. (Ref 4) reported four stages (I: copper dissolves, II: cell membrane ruptures, III: generation of reactive oxygen species (ROS), and IV: genomic and plasmid DNA degradation) of contact-killing of bacteria, yeasts, and viruses on the Cu touch surfaces. In stage I, copper ions form by oxidation and dissolution and diffuse into the surroundings where they are then transported to the cell membrane either by donor ligand receptors or by direct adhesion. Some of the released copper ions may be used by the cell for its physiological function; but the excessive copper ions trigger preventative mechanisms in several ways such as ions outflux, isolation and extrusion of matrix ions, and using external proteins to entrap harmful ions to avoid damaging the cell membrane and its internal structures (Ref 5). The surplus copper ions break the cells and release the cytoplasm in stage II. The breakage of the cell membrane ensures continuous copper ions influx which leads to the formation of ROS by redox reactions which further irreversibly damage the cell membrane and the internal structures. In stage IV, the copper ions reach the DNA through the cell and degrade it by reacting with ROS.

A bacteria disinfection study on copper and non-copper surfaces was conducted in a hospital for 5 weeks (Ref 6). The remaining median numbers of microorganisms were found to be less than 10% (i.e., over 90% disinfection rate) on copper-containing surfaces compared to their control equivalents. The other factors such as patinas and thin oxide layer formation on copper surfaces do not appear to affect the antimicrobial efficacy. Furthermore, the effectiveness is more prominent in a dry condition where Cu(II) oxide can form than in the wet environment where Cu(I) is present (Ref 7, 8). The surface cleaning also does not affect the Cu antimicrobial properties (Ref 7). The biocidal efficacy of Cu depends on the Cu content in the alloys/coatings, 100% Cu-containing surface works best for disinfection; however, 60% Cu is set as a minimum threshold for the maximum toxicity as reported in (Ref 1, 9).

Cold spray (CS) technology is a powerful powder consolidation process for coating development as well as for dimension restoration and repair applications (Ref 10, 11). The CS process is a solid-state powder particle consolidation process that utilizes powder feedstock transported using a heated carrier gas (either N_2 or He) through a convergent–divergent de Laval nozzle with a supersonic velocity impacted on a substrate. One of the two main bonding mechanisms in the CS is mechanical interlocking by severe plastic deformation and the other one being metallurgical bonding. Upon impacting powder particles on a metallic substrate, severe local deformation creates mechanical interlocks by means of adiabatic shear instability and materials jetting (Ref 12, 13). Moreover, the high impact breaks the surface oxide layer of powder and substrate, putting fresh metal surfaces in contact which may in turn result in metallurgical bonding. In addition to coating development and repair applications (Ref 14), the CS process has the potential to produce free-forming parts by using the layer-by-layer deposition method, known as cold-spray additive manufacturing (CSAM) (Ref 11, 15-17). Properties of the CS-deposited coating depend on various processing and powder/substrate properties. The feedstock powder particles play an important role in coat quality; particle size ranging from 10 to 100 μm is suitable for CS deposition. A wide range of materials can be utilized as a cold spray powder feedstock: Cu, Al, Ni, Ti, steel, Ni-based superalloys, composites, etc. For a successful powder consolidation, the particles must reach a range of velocity called critical velocity at which powder adheres to the substrate; under or over the critical velocity range, the particles rebound or erode the substrate, respectively (Ref 18). The typical velocity range achieved by using various powder particles is ranging from 300 to 1200 m/s.

A thorough literature survey suggests a very limited study on the bonding mechanism of CS-deposited metallic particles to the polymeric substrate. An investigation carried out by Sturgeon et al. (Ref 19) reported a successful coating deposition (with low porosity) of aluminum particles on carbon fiber-reinforced PEEK substrate after appropriately designing the spray nozzle, working pressure, gas preheating, and higher stand-off distance. The outcomes of the study highlight a good contact between the particles and the adjacent polymer matrix; however, the interface was found to be porous with strands of polymer bridging across the coating. The porosity on the coating is mostly located at the less deformed particles' boundaries. The comparative effect of gas temperature and pressure on CS deposition of single Cu particle on PEEK substrate was studied by Chen et al. (Ref 20). Their study suggests a deeper Cu particle penetration and jet formation around the particle on the PEEK substrate with increasing gas pressure. It is evident that higher particle velocity (due to the high gas pressure) results in a higher particle penetration or mechanical interlocking and thermal softening (kinetic energy converted to heat-induced softening). The particle's velocity will increase at higher gas pressure which would provide higher thermal softening on the substrate. However, the severity of the thermal softening depends on the respective hardness of the sprayed particles and substrates. For a successful mechanical interlocking during the deposition, the substrate surface damage is necessary which can only be achieved by a combination of suitable temperature and pressure. The effect of gas temperature of Cu particle

deposition on the polymeric substrate was investigated by Che et al. (Ref 21). The finding indicates that for thermoplastic substrates, the particle's temperature higher than glass transition temperature (Tg) can provide deeper particle penetration and better particle/substrate interlocking.

SARS-CoV-2 virus inactivation capability of the CS-coated Cu surface on stainless steel substrate was studied by Hutasoit et al. (Ref 22). Here, 96% virus inactivation within 2-h and 99.2% in 5-h were achieved on Cu-coated surfaces compared to the bare stainless steel. The study conducted by Champagne et al. (Ref 23) shows that the cold spray deposited coating provides superior antimicrobial properties compared to the coating prepared by plasma and wire arc thermal spray techniques. The supersonic velocity of powder particles in the cold spray process produced a highly dense coating structure with increased dislocation density which offers higher ionic copper diffusion (Ref 23). Thus, the improved antimicrobial effectiveness has resulted from the high degree of dislocation density generated by the process of high particles' tamping. The role of copper oxides generated by wet oxidation (CuO) or by atmospheric contamination (Cu_2O, which may be generated in the cold spray process as well) on bacteria contact killing was studied by Hans et al. (Ref 24). Their study confirms that CuO inhibits bacteria contact killing significantly, whereas no influence of Cu_2O was observed; moreover, Cu_2O works like a pure copper material. Their study also suggests that the thermally generated oxide during the cold spray process does not affect the viral inactivation mechanism. The intrinsic features of cold spray deposited coating such as dense microstructure, low porosity, and high density of dislocation improve antimicrobial efficacy as reported by Sundberg et al. (Ref 25). The surface roughness and percentage of grain boundaries are the two factors that influence copper contact killing mechanism. Greater surface roughness implies a large number of grain boundaries as well as more area for virus/bacteria reservoir (Ref 26). The effect of surface roughness on nano-structured and conventional cold spray deposited

coating was studied by Sundberg et al. (Ref 27). Their study suggests a greater reduction of Influenza A virus on nanostructured Cu coating over conventional Cu; however, both coated surfaces appeared to be equally effective against MRSA after 2 h of exposure. A larger scale of surface roughness (over 0.1 mm^2) has a lower contact-killing rate due to the percentage reduction in grain boundaries and large reservoir for virus storage. Higher surface roughness is not always effective to have higher contact-killing because the ionic diffusion of copper depends on the number of grain boundaries. Nanomaterial Cu-coated surface with low surface roughness but a larger number of smaller grains provide better contact-killing due to the increased in ion flow (Ref 28, 29).

The overarching goal of this research is to reduce the risk of COVID-19 and infectious diseases transmission through common/shared public surfaces. The focus of this work is on developing optimum coating parameters and conditions for onsite cold spray copper coating on common surfaces made of rubber or rubber-like materials.

Materials, Methods, and Processes

Materials and Cold Spray Process

Pure irregular-shaped Cu feedstock powder was provided by Centerline Ltd., (Windsor, ON, Canada), catalogue no. SST-C5003. The external synthetic rubber part of a polyurethane-based escalator handrail (Shanghai Xiangshang Co. Ltd., China) was used as the substrate for cold spray deposition as shown in Fig. 1. The substrates surface was cleaned with ethanol before the coating deposition.

The CS coating was developed using the Supersonic Spray Technologies (SST™) Series P CS system manufactured by Centerline Ltd., (Windsor, ON, Canada). The deposition took place at a nozzle stand-off distance of 25 mm and a 90° deposition angle. The nozzle speed was 100 mm/s with 0.5 mm offset to obtain continuous coating

Fig. 1 (a) a section of handrail rubber (6 inches length) cut from a long piece, (b) the flat rubber samples prepared for coating, and (c) Cu-coated rubber and bare substrate surface
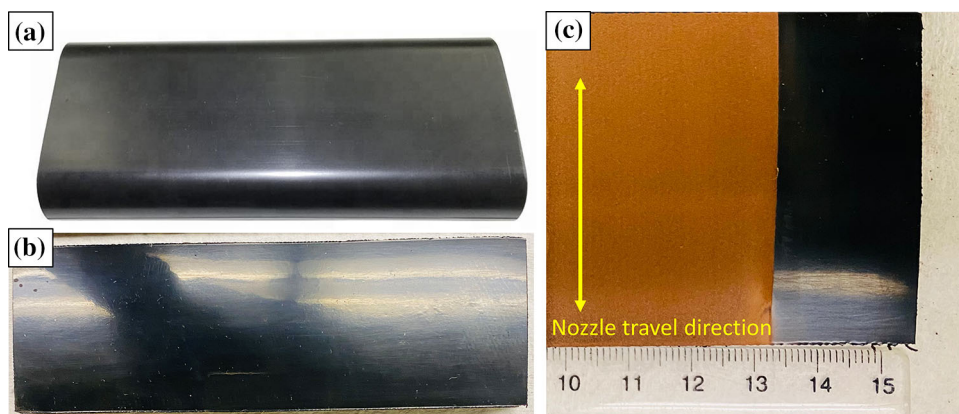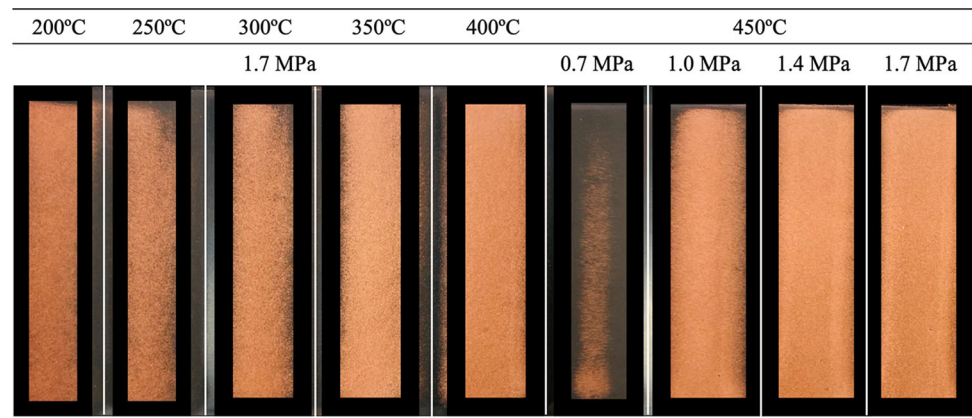
Fig. 2 Cu-coated rubber surfaces obtained using different combinations of temperature and pressure

layer on the entire surface of the substrate as shown in Fig. 1(c). Nitrogen was used as the process gas at temperatures, pressures, and feed rates varied from 200 to 450 °C, 0.7 to 1.7 MPa, and 10-20 gm/min, respectively (Fig. 2). The process parameters were selected based on the coating adhesion, uniformity, and maximum coverage. Out of several tested process parameters, a 450 °C temperature, 1.7 MPa pressure, and 20 gm/min feed rate were considered as the best process parameters for a superior coating quality. From Fig. 2, it can be identified that the higher gas temperature and pressure combination gives the best coating quality. Among the two parameters (i.e., temperature and pressure), the temperature seems to have more influence on the coating quality as reasonable coat quality was not obtained under 400 °C at 1.7 MPa, the higher the temperature the better the coating uniformity. Single- and double-pass coated specimens were prepared for antimicrobial and virucidal activity tests. To assess the adhesion of copper on rubber substrate, a simple bend test (folding the coated soft rubber section into U-shape, see the video of this test in the supplementary file provided for the online version) was performed. After several folding/unfolding tests, the coating surface remained undamaged, showing no signs of breakage on the coating surface. To achieve a single particle impact on the rubber surface, a combination of the highest nozzle speed and lowest powder feed rate was considered.

Feedstock powder particle size distribution and volume fraction were estimated using CAMSIZER-X2 (RETSCH Technology, Germany) where the particle sizes and shapes information are measured (range 0.8 μm to 8 mm) based on the dynamic image analysis principle. The morphology of powders and the cross section of the coated samples were analyzed using a field-emission scanning electron microscope (FESEM, Zeiss LEO 1530 and Zeiss Ultra-Plus). The samples for metallography were cold mounted and mechanically ground and polished to 0.25-μm diamond suspension. The polished samples were gold-coated before SEM observation. Phase identifications of the powder particles and the substrates were carried out using a Bruker D8-Discover x-ray diffraction (XRD) equipped with a VÅNTEC-500 area detector and Cu-Kα radiation (λ = 1.5406 Å) at an operating voltage and current condition of 40 kV and 40 mA with 2theta range from 20 to 120°. The crystallite size was estimated by measuring differences between the FWHM of XRD peaks from the coating and the FWHM of XRD peaks from the copper particles. Noting that the investigated Cu powder was produced using the electrolysis process, therefore, it can reasonably be considered as stress-free Cu particles.

Viricidal Activity Tests

A human seasonal coronavirus surrogate for SARS-CoV-2, human coronavirus 229E (HCoV-229E; ATCC VR-740) was propagated on MRC-5 (ATCC CCL-171) cells (Cedarlane, Burlington, ON, Canada). A recombinant baculovirus (*Autographa californica* multiple nucleopolyhedrovirus) engineered to express the fluorescent protein mKOk under the p10 promoter was amplified utilizing Sf-9 insect cells (Sf9, ATCC CRL-1711). MRC-5 and Sf9 cells were maintained in Eagle's minimum essential medium (EMEM) supplemented with 10% (vol/vol) fetal bovine serum (FBS) (Wisent BioProducts, Saint-Jean-Baptiste, QC, Canada) and Gibco Sf-900III (Thermo Fisher Scientific, Waltham, MA, USA), respectively. MRC-5 cells were maintained by serial passage in cell culture-treated T flasks (Thermo Fisher Scientific) at 37 °C in a humidified atmosphere under 5% CO_2 in air. Sf9 cells were maintained in 125 mL glass shake flasks (Corning GlassWorks, Corning, NY, USA) with a working volume of 25-30 mL at 27 °C and agitated at 130 rpm.

HCoV-229E is a human pathogen which causes mild upper respiratory disease and is structurally similar to SARS-CoV-2 (Ref 30, 31). HCoV-229E is classified as a Risk Group 2 pathogen, which allows for ease of laboratory use in comparison with SARS-CoV-2 (Risk Group 3);

HCoV-229E has been utilized as a surrogate for SARS-CoV-2 inactivation in a variety of applications (e.g., UV-C disinfection (Ref 32), contact lens solution disinfection (Ref 33), and antiviral coating disinfection (Ref 34). HCoV-229E working stock was produced by infecting 80-90% confluent MRC-5 cells at a multiplicity of infection (MOI) of 0.01 and incubating at 33 °C until cytopathic effects were observed to have progressed through 80% of the cell monolayer (approximately 5 days). Supernatant was harvested, centrifuged at $1000 \times g$, and stored at -80 °C until use. The effects of the copper-coated surfaces on baculovirus inactivation were tested for the purpose of method development due to its ease of use in comparison with human coronaviruses, and also due to the ability to demonstrate a higher degree of inactivation provided by a higher titer virus stock (Ref 35). Baculovirus working stock was produced by infecting Sf9 cells at a density of 1.5×10^6 cells/mL at an MOI of 0.01 and incubating for 72-96 h until cell viability dropped to 80%. Cell culture supernatant was harvested and centrifuged at $1000 \times g$ to remove cells and cell debris. Baculovirus working stock was stored at 4 °C until use. HCoV-229E was propagated in EMEM supplemented with 2% FBS (vol/vol) while baculovirus was propagated in Sf-900III. Working stock titers were approximately 4×10^5 MPN/mL and 7×10^8 MPN/mL for HCoV-229E and baculovirus, respectively.

Infectious viral titer was determined via end-point dilution assay (EPDA) in 96-well plates (12 wells/dilution), utilizing tenfold serial dilutions and an inoculation volume of 10 μL/well. EPDAs were performed utilizing MRC-5 cells and Sf9 cells for quantification of HCoV-229E and baculovirus, respectively. Wells were scored as positive or negative for virus after 7 days based on the presence or absence of cytopathic effects (HCoV-229E) or red fluorescence (baculovirus). Viral titer was quantified utilizing the most probable number (MPN) estimation (Ref 36). The limit of detection represents the lowest calculable viral titer (i.e., one positive well).

Virucidal activity testing was performed by depositing 25 μl droplets of virus working stock on bare rubber control, single-pass Cu-coated, and double-pass Cu-coated surfaces. The samples were kept in a humidified box to prevent droplet evaporation over the course of the surface exposure. At the appropriate time point (i.e., 2, 4, or 8 h), the 25 μl virus-containing droplet was removed from the surface and diluted into virus propagation media. The surface was then repeatedly washed by vigorous pipetting of fresh virus propagation media to remove any adhered virus. These washes were added to the sample for a final surface-exposed droplet dilution of 1 in 10. Samples were then immediately serially diluted, and EPDAs were

performed. Droplets were deposited, recovered, and titered in triplicate for each condition tested.

Cytotoxicity and neutralization control experiments were performed to ensure that dilution during droplet resuspension was sufficient to prevent the Cu in solution from causing cytotoxic effects during titration and from causing viral inactivation after droplet removal from the surface. Cytotoxicity controls were performed identically to the testing except the droplets consisted of virus propagation media instead of virus working stock. Neutralization control experiments were performed in the same manner as cytotoxicity control experiments, with the addition of virus to the samples occurring after droplet removal and surface washing. The virus-spiked samples were then incubated at 4 °C overnight prior to titration via EPDA. All cytotoxicity controls showed no cytotoxic effects for MRC-5 and Sf9 cells. All neutralization controls did not show significant viral titer reduction after droplet recovery and dilution for both HCoV-229E and baculovirus, indicating that dilution was sufficient to neutralize the Cu in solution and avoid false results due to an extension of the incubation period.

Antimicrobial Activity Tests

*Escherichia coli (*ATCC 10,798*)* was acquired from Cedarlane Laboratories (Burlington, ON, Canada). The bacteria were inoculated separately in sterile nutrient broth, prepared according to the supplier's (Sigma-Aldrich) instructions. The broth was incubated for a period of 12 h at 37 °C, and after cultivation, the bacterial suspension was centrifuged and washed twice using 10 mM of sterile phosphate buffered saline (PBS) at pH 7.4. The turbidity of the bacterial concentrations was adjusted to an optical density (OD_{600}) of 0.2 at 600 nm, corresponding to 10^8 cfu/mL, using a Hewlett Packard 8453 UV–visible spectrophotometer. The concentration of the viable microbial cells was also verified using the heterotrophic plate count method after preparing appropriate dilutions of the bacterial culture. Prior to the antimicrobial testing, the samples were placed in 1% detergent solution (Liquinox) for 2-4 h, then rinsed thoroughly with deionized water and allowed to dry. The surfaces were removed with the help of forceps and placed in a petri dish and left to dry in a biosafety cabinet overnight.

To assess contact killing on the coated surfaces, a version of the EPA protocol for hard non-porous copper-based antimicrobial surfaces was used, as followed in (Ref 37). Inoculum preparation was performed by adding soil load composed of both protein and carbohydrate to mimic a contaminated natural environment. The soiling solutions were comprised of bovine serum albumin at 50 mg/ml,
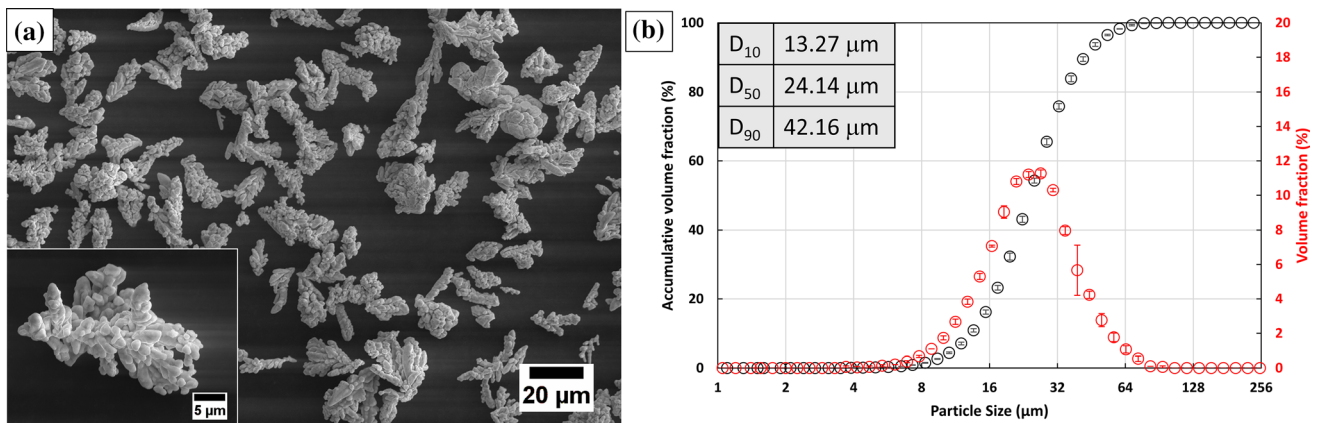
Fig. 3 (a) SEM micrograph of the irregular-shaped pure Cu powder with inset a magnified single particle, (b) powder particles size distributions and cumulative volume fraction
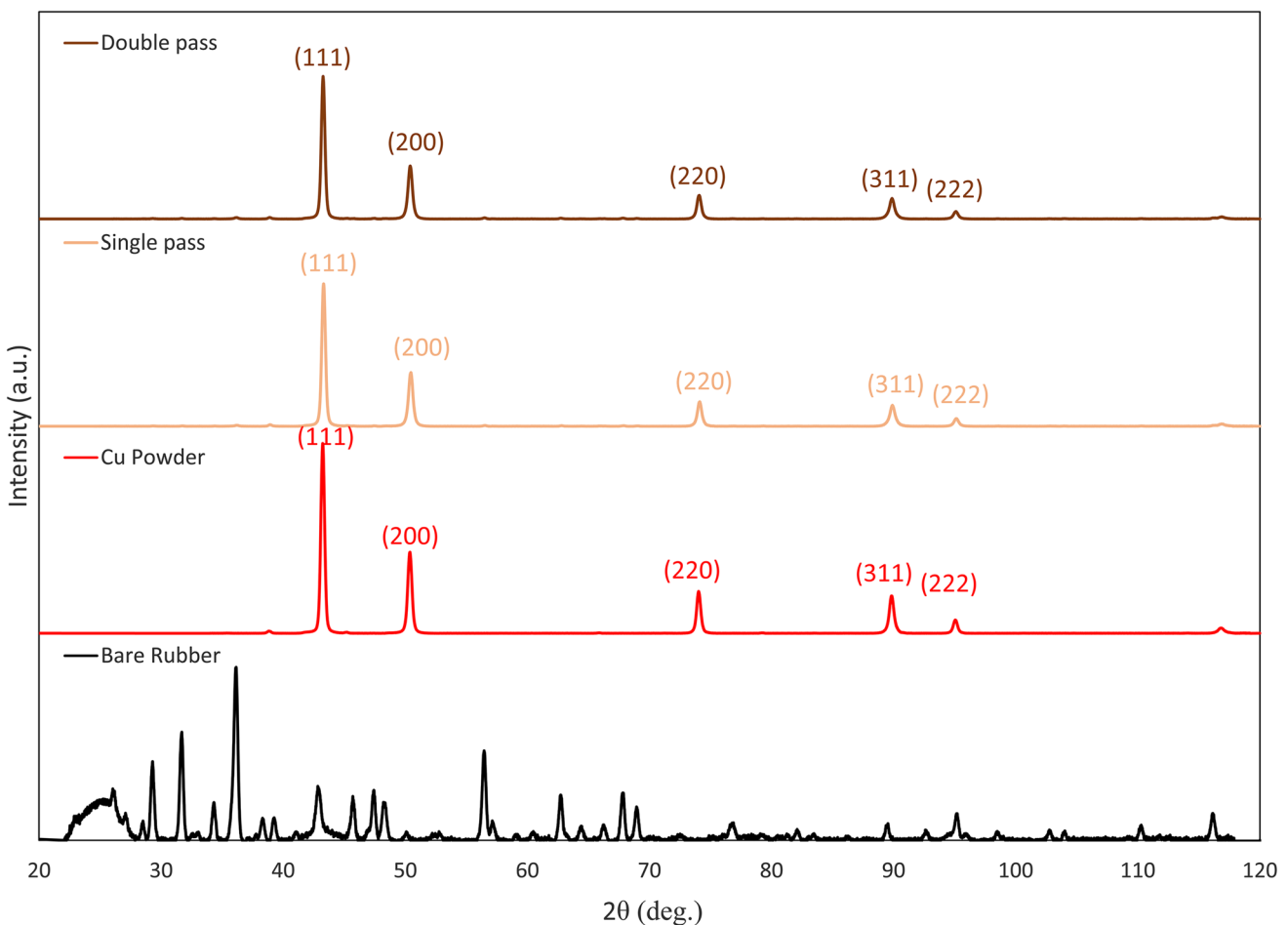

Fig. 4 X-ray diffraction patterns of synthetic bare rubber, Cu powder, single- and double-pass Cu-coated surface

yeast extract at 50 mg/ml, mucin at 4 mg/ml and passed through a 0.2-μm pore diameter membrane filter independently. The stock solutions of the soil load solutions were prepared fresh every time. A 160 μl aliquot of simulated load comprised of 25 μl bovine serum albumin, 35 μl yeast extract, and 100 μl mucin were added to 340 μl of the

bacterial suspension of interest, vortexed, and 20 μl spread across the test surfaces of inch-square (6.5 cm^2) and left at room temperature for 2 h. The test surfaces were placed inside a sterile petri dish. Then, the test surface was placed into a 50-mL beaker with the help of sterile forceps. Afterward, 20 mL of sterile PBS was poured onto the

Fig. 5 SEM micrographs of as-sprayed Cu coating surfaces (a and c) and cross-sectional views (b and d), where (a) and (b) show single pass, and (c) and (d) show double-pass results (Color figure online)
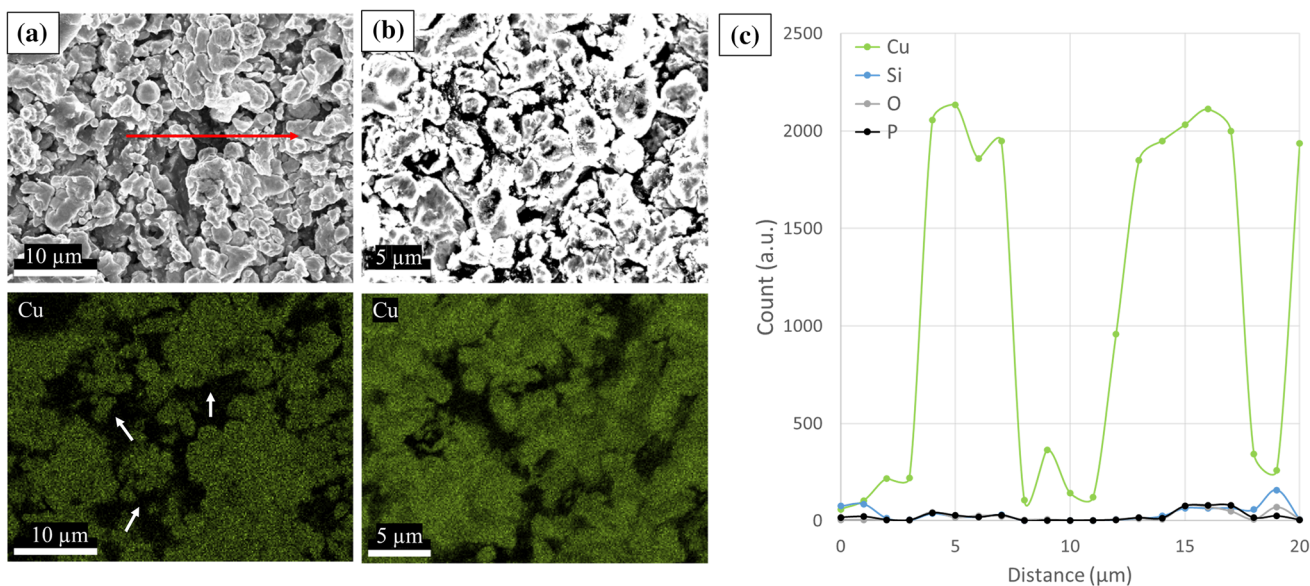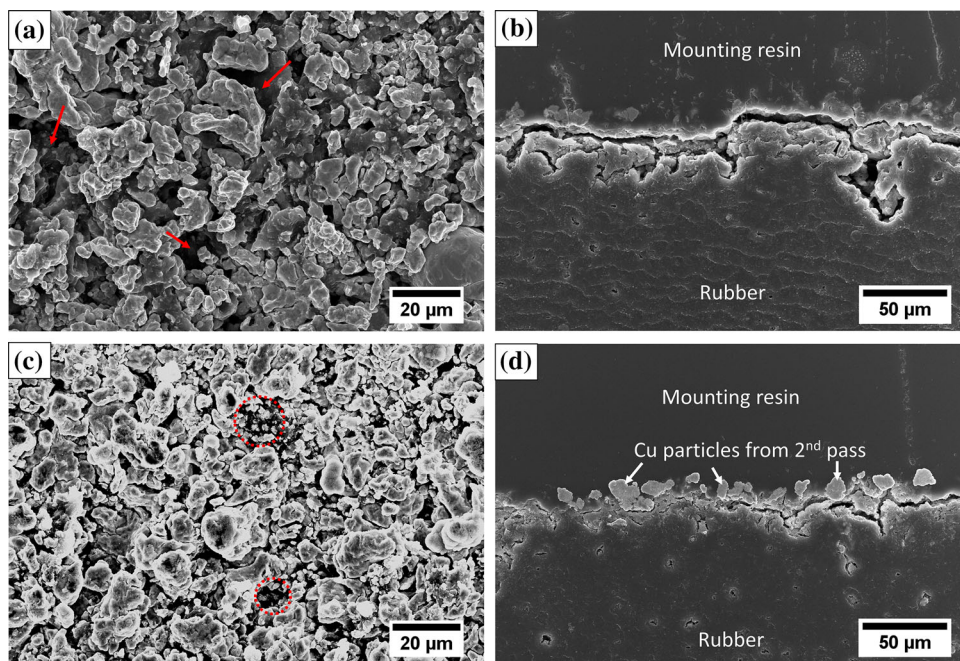

Fig. 6 EDX mapping for Cu distribution on coating surfaces, (a) single pass, (b) double pass, and (c) line scan of Cu, Si, O, and P on the single-pass coating surface, as shown by the red arrow in (a) (Color figure online)

surface, and this was sonicated for 5 min at 45 kHz for the recovery of bacteria. The recovered solution was then further serially diluted three times (i.e., dilution factors of 10^1, 10^2 10^3). Then, 0.1 mL of undiluted and each dilution were spread onto plate count agar. Plates were incubated at 37 °C for 48 h, then colonies were counted. Each experiment was replicated 3 times for single and double pass. The log reduction for test surfaces was recorded relative to rubber control sample. The results are shown as mean values, and error bars correspond to standard deviations

(SD) of the mean values of results obtained from the three independent repeat experiments.

Results

Powder Characterization

Figure 3 shows the SEM images and particle size distribution of the used irregular-shape pure Cu (> 99.7%) powder produced by the electrolysis method (Ref 38). The

Fig. 7 EDX mapping for Cu distribution on coating cross sections, (a) and (b) single pass, (c) and (d) double pass
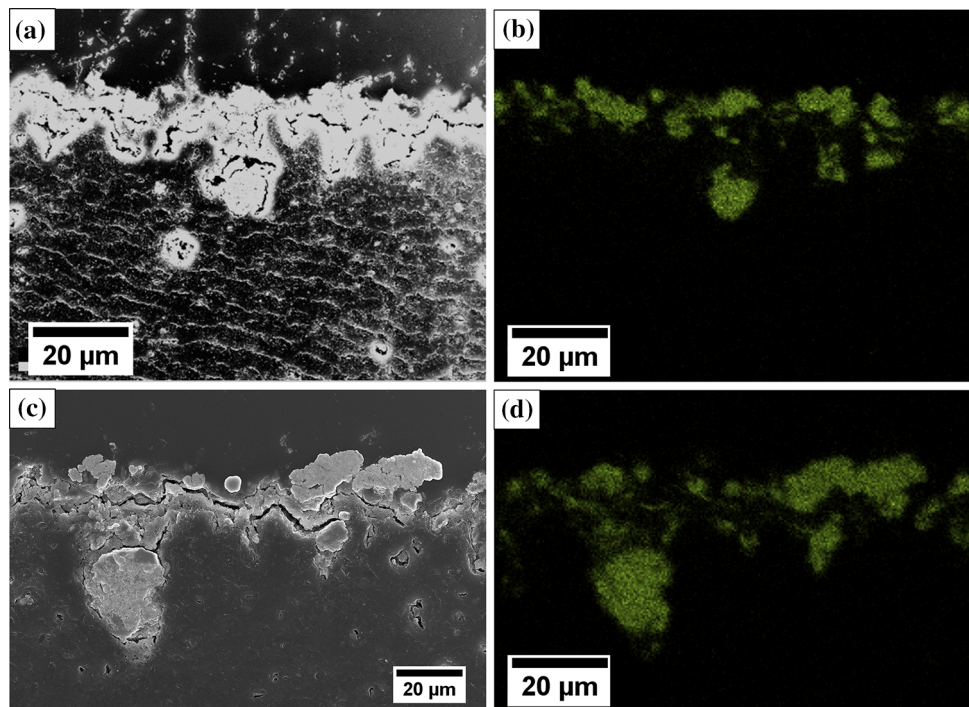
powder exhibits cauliflower-like dendritic morphology with an average particle size of about 24 μm and a size distribution ranging from 13 (D_{10}) to 42 μm (D_{90}) (Fig. 3). It can be seen that the thick secondary dendritic structure grows on the trunk. The irregular-shape powder particles with tailored size distribution were specially designed by the company for maximum velocity. Being irregular-shaped, the powder particles provide superior mechanical interlocking with all types of substrate conditions, hence considered for the rubber substrate. When studying the CS-deposited Cu coating for antimicrobial and antiviral applications, two factors were taken into consideration: the percentage of grain boundaries, and surface area. A larger grain boundary area results in a greater Cu ion diffusion for maximum disinfection efficacy (Ref 39). The coat surface quality is a direct indication of overall surface area; rougher surface would provide a higher surface area hence improved virus/bacteria inactivation. The irregular-shape powder is considered the best-suited powder for this research due to its higher grain boundaries and surface areas.

Coating Characterization

Figure 4 shows the XRD patterns for bare rubber, powder, and coat surfaces. The bare rubber surface exhibits typical synthetic rubber characteristics, whereas all other patterns for Cu powder and coat surfaces are showing only common Cu (111), (200), (220), (311), and (222) peaks without any

oxide or other species implying full substrate surface coverage. To understand how the particle crystallite sizes have changed during the deposition process, the average crystallite size of the Cu powder and the deposited coatings was estimated using the Scherrer equation (Ref 40). It was found that the average full width at half maximum (FWHM) increased from 0.4016° to 0.4166°. (single pass), and 0.4122°. (double pass) suggesting refinement of the crystallite size which is expected due to the high-velocity impact and particle deformation in the coating form. However, the crystallite size in the coating was not significantly different than in its powder form which implies limited/no deformation as the substrate is the soft rubber material. It was also noted that there were no appreciable crystallite size differences between the single-pass (337 ± 78 nm) and double-pass (349 ± 82 nm) coatings.

Figure 5 shows SEM examination of coating top surfaces and cross-sectional micrographs for single- and double-pass coatings. It can be seen from Fig. 5(a) and (c) that the Cu particles completely covered the rubber surface although more coverage was found on the double-pass coated surface. On the single-pass coated surface, some darker areas can be identified [pointed with red arrows in Fig. 5(a)] which may not be covered with Cu particles fully or particles may not adhere entirely. When the identical darker regions [highlighted with red circles in Fig. 5(c)] are traced on the double-pass coated surface, smaller fragmented particles can be found in these regions suggesting double-pass coating has better coverage than the single pass. The cross-sectional views revealed

Fig. 8 (a) HCoV-229E and (b) baculovirus inactivation over time of droplet exposure to rubber and copper-coated rubber surfaces. All conditions were tested in triplicate, and error bars represent the range of the data. Downward arrows indicate no detectable virus for that time point. Zero-time point is the starting titer of the virus, not deposited as a droplet (i.e., working stock titer)

(a)

(b)
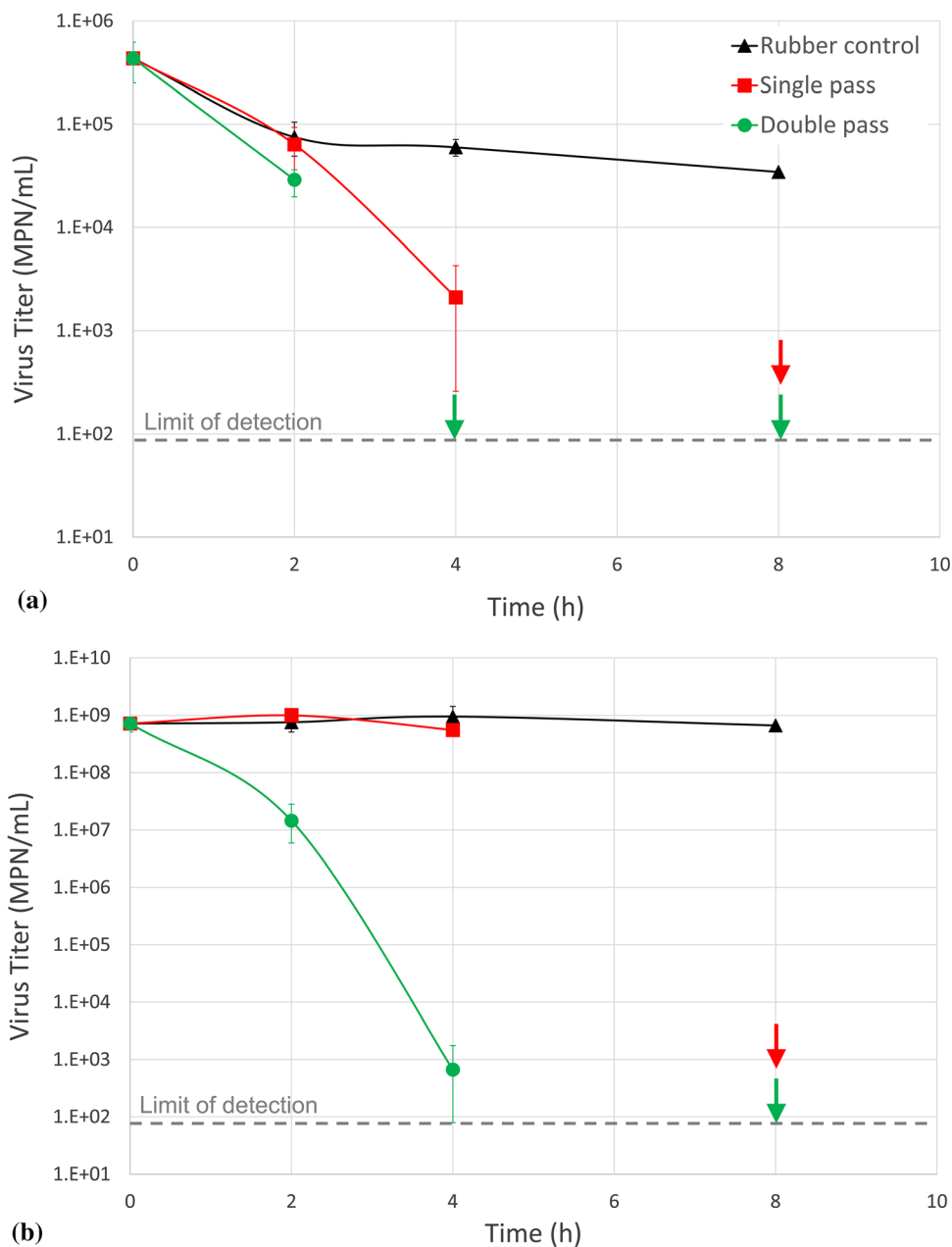
complete particle penetration into the rubber substrate in the single-pass condition (Fig. 5b), whereas additional protruded powder particles can be observed on top of the penetrated particles in the double-pass condition (Fig. 5d). It is also noted that the maximum penetration depth of the powder particle is higher (around 40 μm) than the average particle size (24 μm) suggesting complete penetration of single particles. Most of the particles from the second pass keep their original size and morphology after impacting on top of the first pass which kind of suggests that the second-pass particles have less degree of penetration/deformation. It is also interesting to see that the second-pass particles did

not remove the first pass as it remains firmly anchored to the rubber substrate.

To understand the overall surface coverage by copper powders, the Cu surface mapping was performed using an energy-dispersive x-ray spectroscopy (EDX) as shown in Fig. 6(a) and (b). An improved Cu coverage was identified on the double-pass sample, i.e., densification of Cu powder increases with a number of depositions pass. There are a number of less Cu covered areas [highlighted with small arrows in Fig. 6(a)] on the single-pass surface which was further investigated using the EDX line scanning by performing a scan through the darker region, highlighted with

a red arrow. The line scan result is shown in Fig. 6(c); it can be seen that Cu is the main constituent in the entire surface, and even the darker region is rich in Cu. Additional Cu maps were performed on the cross-sectional samples as can be found in Fig. 7. Cu element almost completely covered the substrate/coating interface as well as penetrated the rubber substrate. Some of the particles completely penetrated the rubber substrate without having any particle/particle bonding. The original shape and size of the particles also remained unchanged; however, more Cu particles appeared to be present at the double-pass coated interface. The total penetration depth into the rubber substrate is higher in the double-pass condition.

Virucidal Activity Results

Exposure of HCoV-229E-containing droplets to the copper-coated surfaces resulted in significant virus inactivation relative to an uncoated rubber surface. Exposure to a double-pass coated surface resulted in no detectable virus after 4-h exposure (> 2.9-log inactivation), while exposure to a single-pass coated surface resulted in approximately 1.5-log inactivation after 4 h, and no detectable virus after 8-h exposure (> 2.6-log inactivation). There was some virus loss over time on the rubber control surface, inactivation numbers stated here are relative to the rubber control surface at each time point (Fig. 8).

Exposure of baculovirus-containing droplets to the copper-coated surfaces also resulted in significant virus inactivation relative to an uncoated rubber surface. A double-pass coated surface showed significant virus inactivation after 2 h (approximately 1.7-log) and 4 h (approximately 6.2-log), and there was no detectable virus (> 6.5-log inactivation) after 8 h. A single-pass coated surface required longer times for virus inactivation, achieving > 6.5-log inactivation after 8-h exposure to the surface. The bare rubber control surface did not result in virus inactivation over the course of the 8-h exposure time (Fig. 8). This significant baculovirus inactivation is in line with a similarly studied copper-nickel-zinc surface (Ref 41).

Antimicrobial Activity Results

A study of the disinfection effectiveness of single- and double-pass cold spray Cu-coated surfaces was performed. The antibacterial properties of two Cu-coated surfaces were assessed against *E. coli*. The viable counts of recovered cells from rubber at different time points were approximately 10^5 cfu/mL. The maximum log reduction calculated for both the single- and double-pass coated
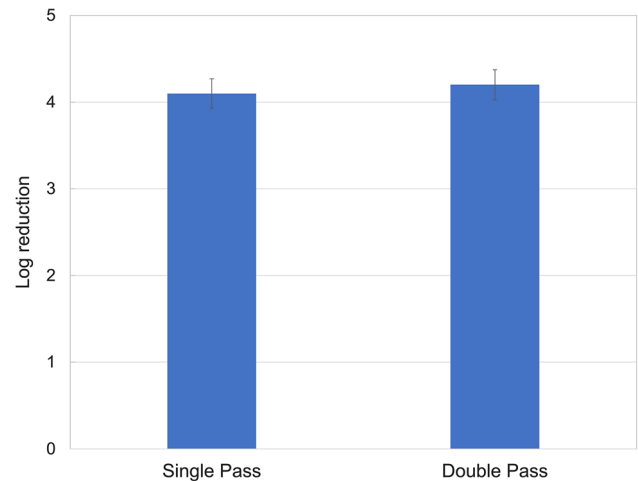

Fig. 9 Antibacterial efficacy of Cu-cold spray coated (single and double pass) samples against *E. coli* after 2 h. (data represent average value of log reduction of viable counts of recovered bacterial cells relative to uncoated rubber control)

samples was around 4-log relative to uncoated controls, which is equivalent to 99.99% reduction of viable *E. coli* in the 2-h period. Recent studies demonstrated that *E. coli* cells were completely inactivated on copper-coated surfaces within one hr (Ref 42, 43). Antimicrobial assay methods and conditions can vary, and in this study, the assays were performed with the inclusion of soiling load not used in some studies. This potentially led to a decrease in log reduction of *E. coli* relative to values mentioned in the literature (Ref 42-44) but still sufficient to be called an effective antimicrobial surface.

Discussion

The early stage of metallic particle impingement onto the polymeric substrate leads to thermal softening due to heat dissipation. Both the temperature and pressure play a vital role on successful coating deposition. In the current investigation, it is confirmed that the higher the gas temperature, the better the coating adhesion. Moreover, the Cu particle penetration depth increases with increasing temperature, pressure, and the number of coating passes. It was interesting to notice that the second-pass particle did not remove the first layer rather increased the particle penetration and number of protruding particles. The first-pass particles were firmly anchored and helped adhering upcoming particles by filling the less covered Cu-containing regions [highlighted with arrows in Fig. 5(a)]. The purpose of the current investigation is to obtain reasonable coating coverage to have a higher disinfection rate rather to produce a thicker coating for structural application. For virus/bacterial disinfection, surface coverage is more

Fig. 10 SEM images showing copper particles penetrated onto rubber substrate, (a) top surface view of a single particle, and (b) cross-sectional view of the identical particle
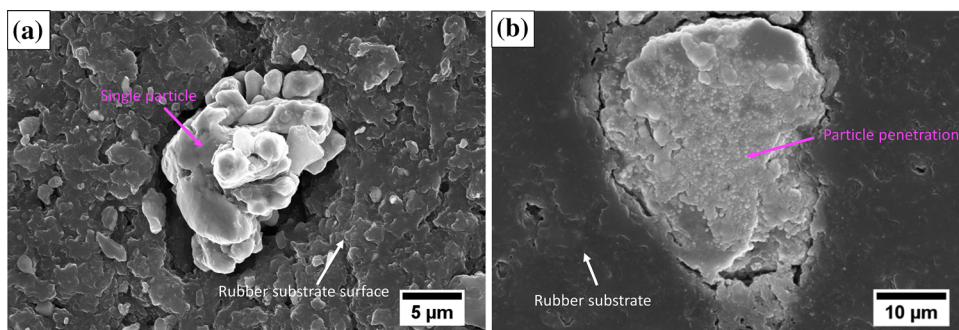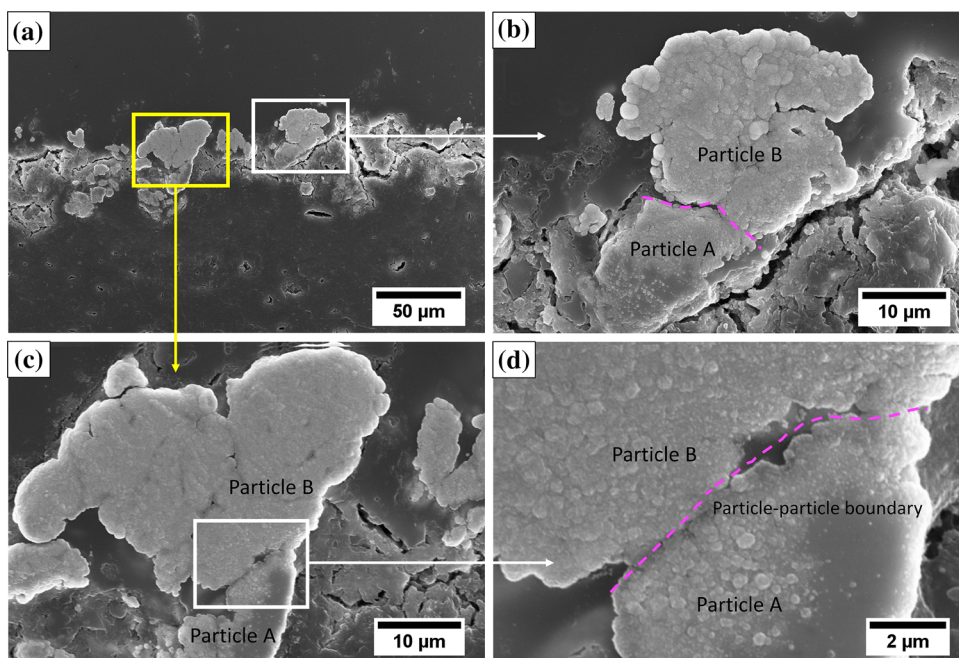

Fig. 11 SEM micrographs of double-pass coated interface showing the enlarged view of particle/particle bonding mechanism

important than the thickness of the coating; therefore, a little attention was paid on fabricating thicker coating.

To confirm the particles' bonding mechanism during the deposition, a single particle impact study was performed as presented in Fig. 8. As can be seen in Fig. 8(a), the irregular-shaped single particle impacted the rubber substrate and made a purely mechanical interlock without showing any particle breakage or deformation due to the soft substrate material. Pure mechanical interlocking between the powder particles and substrate was achieved by using the high particle impact velocity. Overall the copper particles experienced very limited deformation (no flattening) which is in accordance with other studies as reported in references (Ref 19, 21, 45). Che et al. (Ref 21) investigated single spherical Cu particle bonding mechanisms on several different polymeric substrates such as CFRP (carbon fiber-reinforced polymer), ABS (acrylonitrile butadiene styrene), PEEK (polyether ether ketone), and PEI (polyethylenimine). The Cu particles did not show any significant plastic deformation on all the studied polymeric substrates. As found in the present investigation, Che et al. (Ref 21) also did not notice any splat formation by severe particle deformation rather particles penetrated and adhered to the substrate. To achieve better particle–substrate adhesion, the substrate surface needs to be damaged by the particle impingement; but erosion may happen due to the excessive substrate damage (Ref 21).

A magnified view of the particle/particle boundary at the interface of the double-pass coated specimen is shown in Fig. 9. Particle A at the interface is a part of the coating that formed during the first-pass deposition, and particle B is from the subsequent second pass. The particle/particle boundary exhibits no plastic deformation as particle B did not show any flattening. It appears to be particle B is anchored to the less Cu covered area of the substrate by mechanical interlocking (Fig. 10). However, after the second-pass deposition, the coating thickness increases, and greater particle penetration was achieved which may provide additional ionic diffusion and result in a greater virucidal and antimicrobial efficacy as shown in Fig. 8 and

9. Although, the quantitative measurements of surface roughness on the single- and double-pass coated surfaces were not taken, based on the cross-sectional micrographs presented in Fig. 7 and 11, double-pass coated surface exhibits more Cu-particles protrusions indicating a rougher surface. The effect of surface roughness on bacterial killing on wire-arc deposited Cu alloys was studied by Shafaghi et al. (Ref 46). They demonstrated a better bacteria accumulation around the surface asperities. However, no significant difference in microbial activities was found on the surfaces with low and high surface roughness.

Conclusions

This work aimed to develop cold spray Cu powder coating on rubber substrate with antiviral and antimicrobial properties. This study provides a fundamental understanding of the metallic particle bonding mechanism with the rubber substrate. The major findings of this work are as follows:

- The successful Cu-coated rubber surface was prepared by using a combination of high temperature and high pressure for the low-pressure cold spray deposition system. The optimum parameters using the irregular shape powders were found to be a temperature and pressure of 450°C, and 1.7 MPa, respectively.
- Fully surface coverage was obtained by using a single-pass coating, additional pass increased the coating thickness and improved deeper particle penetration. The particle/substrate bonding was purely mechanical interlocking with no particles' deformation or flattening.
- Excellent virus inactivation was achieved via exposure to a double-pass Cu-coated surface relative to a bare rubber control surface. 2-h exposure resulted in an approximately 1.7-log baculovirus inactivation. 4-h exposure resulted in an approximately 6.2-log baculovirus inactivation and no detectable HCoV-229E (> 2.9-log inactivation). Longer exposure times were required to achieve similar virus inactivation on a single-pass coated surface.
- The single- and double-pass coated Cu coatings show 99.99% disinfection of *E. coli* (4-log reduction versus controls) after 2-h exposure confirming cold spray Cu coating on rubber surface has an excellent antibacterial property.

References

1. S.A. Wilks, H.T. Michels and C.W. Keevil, Survival of Listeria Monocytogenes Scott A on Metal Surfaces: Implications for Cross-Contamination, *Int. J. Food Microbiol.*, 2006, **111**(2), p 93-98.
2. S.L. Warnes, Z.R. Little and C.W. Keevil, Human Coronavirus 229E Remains Infectious on Common Touch Surface Materials, *MBio*, 2015, **6**(6), p e01697-15.
3. N. van Doremalen, T. Bushmaker, D.H. Morris, M.G. Holbrook, A. Gamble, B.N. Williamson, A. Tamin, J.L. Harcourt, N.J. Thornburg, S.I. Gerber, J.O. Lloyd-Smith, E. de Wit and V.J. Munster, Aerosol and Surface Stability of SARS-CoV-2 as Compared with SARS-CoV-1, *N. Engl. J. Med.*, 2020, **382**(16), p 1564-1567.
4. G. Grass, C. Rensing and M. Solioz, Metallic Copper as an Antimicrobial Surface, *Appl. Environ. Microbiol.*, 2011, **77**(5), p 1541-1547.
5. K. Sundberg, Application of Materials Characterization, Efficacy Testing, and Modeling Methods on Copper Cold Spray Coatings for Optimized Antimicrobial Properties, *Worcester Polytechnic Institute*, (2019), https://digital.wpi.edu/show/3n204157n
6. A.L. Casey, D. Adams, T.J. Karpanen, P.A. Lambert, B.D. Cookson, P. Nightingale, L. Miruszenko, R. Shillam, P. Christian and T.S.J. Elliott, Role of Copper in Reducing Hospital Environment Contamination, *J. Hosp. Infect.*, 2010, **74**(1), p 72-77.
7. H.T. Michels, J.O. Noyce and C.W. Keevil, Effects of Temperature and Humidity on the Efficacy of Methicillin-Resistant Staphylococcus Aureus Challenged Antimicrobial Materials Containing Silver and Copper, *Lett. Appl. Microbiol.*, 2009, **49**(2), p 191.
8. A. Mikolay, S. Huggett, L. Tikana, G. Grass, J. Braun and D.H. Nies, Survival of Bacteria on Metallic Copper Surfaces in a Hospital Trial, *Appl. Microbiol. Biotechnol.*, 2010, **87**(5), p 1875-1879.
9. J. Mostaghimi, L. Pershin, H. Salimijazi, M. Nejad and M. Ringuette, Thermal Spray Copper Alloy Coatings as Potent Biocidal and Virucidal Surfaces, *J. Therm. Spray Technol.*, 2021, **30**(1-2), p 25-39.
10. V. Champagne and D. Helfritch, Critical Assessment 11: Structural Repairs by Cold Spray, *Mater. Sci. Technol.*, 2015, **31**(6), p 627-634.
11. S. Yin, P. Cavaliere, B. Aldwell, R. Jenkins, H. Liao, W. Li and R. Lupoi, Cold Spray Additive Manufacturing and Repair: Fundamentals and Applications, *Addit. Manuf.*, 2018, **21**(April), p 628-650.
12. H. Assadi, F. Gärtner, T. Stoltenhoff and H. Kreye, Bonding Mechanism in Cold Gas Spraying, *Acta Mater.*, 2003, **51**(15), p 4379-4394.
13. M. Grujicic, C.L.L. Zhao, W.S.S. DeRosset and D. Helfritch, Adiabatic Shear Instability Based Mechanism for Particles/Substrate Bonding in the Cold-Gas Dynamic-Spray Process, *Mater. Des.*, 2004, **25**(8), p 681-688.
14. V.K. Champagne, The Repair of Magnesium Rotorcraft Components by Cold Spray, *J. Fail. Anal. Prev.*, 2008, **8**(2), p 164-175.

15. D. MacDonald, R. Fernández, F. Delloro and B. Jodoin, Cold Spraying of Armstrong Process Titanium Powder for Additive Manufacturing, *J. Therm. Spray Technol.*, 2017, **26**(4), p 598-609.

16. A. Sova, S. Grigoriev, A. Okunkova and I. Smurov, Potential of Cold Gas Dynamic Spray as Additive Manufacturing Technology, *Int. J. Adv. Manuf. Technol.*, 2013, **69**(9-12), p 2269-2278.

17. S. Pathak and G. Saha, Development of Sustainable Cold Spray Coatings and 3D Additive Manufacturing Components for Repair/Manufacturing Applications: A Critical Review, *Coatings*, 2017, **7**(8), p 122.

18. M. Hassani-Gangaraj, D. Veysset, K.A. Nelson and C.A. Schuh, Supersonic Impact of Metallic Micro-Particles, *arXiv Mater. Sci.*, 2016, **1612**, p 08081.

19. A. Sturgeon, B. Dunn, S. Celotto and B. ONeill, Cold Sprayed Coatings for Polymer Composite Substrates, *Eur. Sp. Agency (Special Publ. ESA SP 2006)*, 2006, **616**, p 1-5.

20. C. Chen, X. Xie, Y. Xie, X. Yan, C. Huang, S. Deng, Z. Ren and H. Liao, Metallization of Polyether Ether Ketone (PEEK) by Copper Coating via Cold Spray, *Surf. Coatings Technol.*, 2018, **342**, p 209-219.

21. H. Che, P. Vo and S. Yue, Investigation of Cold Spray on Polymers by Single Particle Impact Experiments, *J. Therm. Spray Technol.*, 2019, **28**(1-2), p 135-143.

22. N. Hutasoit, B. Kennedy, S. Hamilton, A. Luttick, R.A. Rahman Rashid and S. Palanisamy, Sars-CoV-2 (COVID-19) Inactivation Capability of Copper-Coated Touch Surface Fabricated by Cold-Spray Technology, *Manuf. Lett.*, 2020, **25**, p 93-97.

23. O. Mishchenko, V. Filatova, M. Vasylyev, V. Deineka and M. Pogorielov, Chemical and Structural Characterization of Sand-lasted Surface of Dental Implant Using ZrO$_2$ Particle with Different Shape, *Coatings*, 2019, **9**(4), p 223.

24. M. Hans, A. Erbe, S. Mathews, Y. Chen, M. Solioz and F. Mücklich, Role of Copper Oxides in Contact Killing of Bacteria, *Langmuir*, 2013, **29**(52), p 16160-16166.

25. K.L. Sundberg, B.C. Sousa, C. Walde, S. Mohanty, J.-H. Lee, V.K. Champagne, D.L. Cote, Microstructural Characterization of Conventional and Nanostructured Copper Cold Gas-Dynamic Spray Material Consolidations, J. Biotechnol. Biomater. (2020)

26. S. Mathews, M. Hans, F. Mücklich and M. Solioz, Contact Killing of Bacteria on Copper Is Suppressed If Bacterial-Metal Contact Is Prevented and Is Induced on Iron by Copper Ions, *Appl. Environ. Microbiol.*, 2013, **79**(8), p 2605.

27. K. Sundberg, M. Gleason, B. Haddad, V.K. Champagne, C. Brown, R.D. Sisson and D. Cote, The Effect of Nano-Scale Surface Roughness on Copper Cold Spray Inactivation of Influenza A Virus, *Int. J. Nanotechnol. Med. Eng*, 2019, **4**, p 33.

28. K. Sundberg, C. Walde, B. Sousa, S. Mohanty, J.-H. Lee, V. Champagne Jr. and D. Cote, Microstructural Characterization of Conventional and Nanomaterial Copper Cold Spray Coatings, *J. Biotechnol. Biomater.*, 2020, **10**(4), p 1-7.

29. K. Sundberg, The Effect of Corrosion on Conventional and Nanomaterial Copper Cold Spray Surfaces for Antimicrobial Applications, *Biomed. J. Sci. Tech. Res.*, 2019, **22**(3), p 16753.

30. Y. Chen, Q. Liu and D. Guo, Emerging Coronaviruses: Genome Structure, Replication, and Pathogenesis, *J. Med. Virol.*, 2020, **92**(4), p 418-423.

31. Y.A. Malik, Properties of Coronavirus and SARS-CoV-2, *Malays. J. Pathol.*, 2020, **42**(1), p 3-11.

32. S.J. Boegel, M. Gabriel, M. Sasges, B. Petri, M.R. D'Agostino, A. Zhang, J.C. Ang, M.S. Miller, S.M. Meunier and M.G. Aucoin, Robust Evaluation of Ultraviolet-C Sensitivity for SARS-CoV-2 and Surrogate Coronaviruses, *Microbiol. Spectr.*, 2021, **9**(2), p e00537-21.

33. C. Lourenco Nogueira, S.J. Boegel, M. Shukla, W. Ngo, L. Jones and M.G. Aucoin, Antiviral Activity of Contemporary Contact Lens Care Solutions against Two Human Seasonal Coronavirus Strains, *Pathogens*, 2022, **11**(4), p 472.

34. S. Butot, L. Baert and A.S. Zubera, Assessment of Antiviral Coatings for High-Touch Surfaces by Using Human Coronaviruses HCoV-229E and SARS-CoV-2, *Appl. Environ. Microbiol.*, 2021, **87**(19), p 1-8.

35. C.L. Nogueira, S.J. Boegel, M. Shukla, W. Ngo, L. Jones and M.G. Aucoin, The Impact of a Rub and Rinse Regimen on Removal of Human Coronaviruses from Contemporary Contact Lens Materials, *Contact Lens Anterior Eye*, 2022, **45**(6), p 101719.

36. R. Blodgett, FDA's Bacteriological Analytical Manual, Appendix 2: Most Probable Number from Serial Dilutions, 2010, https://www.fda.gov/food/laboratory-methods-food/bam-appendix-2-most-probable-number-serial-dilutions. Accessed 2 September (2022)

37. S. Cohen, US Environmental Protection Agency, Office of Pesticide Programs, Environ. Prot. Agency, Off. (July), 5-13 (1984) http://www.epa.gov/opp00001/methods/atmpmethods/QC-23-01.pdf

38. W.B. James, Powder Metallurgy Methods and Applications, Powder Metallurgy, P. Samal, J. Newkirk, Eds., ASM International, 9-19. (2015)

39. V.K. Champagne, D.J. Helfritch and M.D. Trexler, Some Material Characteristics of Cold-Sprayed Structures, *Res. Lett. Mater. Sci.*, 2007, **2007**, p 1-3.

40. R.F. Bryan, Worked Examples in the Geometry of Crystals. (Second Edition). By H. K. D. H. Bhadeshia. London: Institute of Materials, 2001. ISBN 0-904357-94-5. Acta Crystallogr. Sect. A Found. Crystallogr. **57**(4), p 478-478. (2001)

41. S.D. Walji, M.R. Bruder and M.G. Aucoin, Virus Matrix Interference on Assessment of Virucidal Activity of High-Touch Surfaces Designed to Prevent Hospital-Acquired Infections, *Antimicrob. Resist. Infect. Control*, 2021, **10**(1), p 1-12.

42. N. Hutasoit, S.H. Topa, M.A. Javed, R.A. Rahman Rashid, E. Palombo and S. Palanisamy, Antibacterial Efficacy of Cold-Sprayed Copper Coatings against Gram-Positive Staphylococcus Aureus and Gram-Negative Escherichia Coli, *Materials (Basel, Switzerland)*, 2021, **14**(22), p 6744.

43. I. Salah, I.P. Parkin and E. Allan, Copper as an Antimicrobial Agent: Recent Advances, *RSC Adv.*, 2021, **11**(30), p 18179-18186.

44. M. Vincent, R.E. Duval, P. Hartemann and M. Engels-Deutsch, Contact Killing and Antimicrobial Properties of Copper, *J. Appl. Microbiol.*, 2018, **124**(5), p 1032-1046.

45. H. Che, X. Chu, P. Vo and S. Yue, Metallization of Various Polymers by Cold Spray, *J. Therm. Spray Technol.*, 2018, **27**(1-2), p 169-178.

46. R. Shafaghi, J. Mostaghimi, V. Pershin and M. Ringuette, Sporicidal Efficacy of Thermal-Sprayed Copper Alloy Coating, *Can. J. Microbiol.*, 2017, **63**(5), p 384-391.